Correlation of Rheology and Light Scattering in Isotactic Polypropylene during Early Stages of Crystallization

N. V. Pogodina, S. K. Siddiquee, J. W. van Egmond, and H. H. Winter*

Department of Chemical Engineering and Department of Polymer Science and Engineering, University of Massachusetts, Amherst, Massachusetts 01003

Received May 8, 1998

ABSTRACT: Structure development during crystallization of isotactic polypropylene (iPP) at low undercooling is studied by small-angle light scattering (SALS) and light transmission. The structure development is related to network formation (gelation) as previously measured on the same sample in dynamic mechanical experiments. Close to the rheologically measured gel point, small-angle light scattering (SALS) patterns in both Hv and Vv modes show circular symmetry; density fluctuations (maximum in Vv invariant) as determined by SALS go through a maximum. Orientation fluctuations develop much more slowly and appear at much later stages of the crystallization process. Growing clusters are characterized by very low anisotropy and low internal crystallinity. The characteristic length scale associated with the cluster at early stages is about 1 μm. At later times, evolution of 2-fold and 4-fold symmetry patterns suggests the development of the anisotropic superstructures. The growth of crystalline clusters leads to a strong increase in turbidity as monitored by light transmission in the Vv mode.

Introduction

The dynamics of crystallization has been extensively studied during the past decade using a variety of techniques including microscopy, SALS, SAXS and WAXD, DSC, FTIR, rheology, etc., and is summarized in excellent reviews.[1−4] Crystallization in polymers is understood to occur through a nucleation and growth mechanism. Chain segments form nuclei of a critical size from which clusters grow, and molecular mobility in the system slows down. Molecular motions become correlated over increasing distances (correlation lengths). At the critical gel point (GP), the correlation length diverges to infinity. Recent time-resolved rheological studies of polypropylene crystallization[5,6] showed that the GP is reached very early in the crystallization process; i.e., the growth rate of a sample spanning network structure is much higher than the crystallization rate. The critical gel is thus soft and consists of a loosely connected network, characterized by a low degree of crystallinity.

Very little is known about the physical origin of the arising connectivity and about the structural characteristics such as their size, shape, anisotropy, and molecular arrangement of the growing clusters. Light scattering is a classical method for studying structure development during crystallization and phase separation processes.[7−9] Although small-angle light scattering (SALS) experiments have been reported for crystallizing polypropylene[10] and polyethylene,[11] these studies were performed at high degrees of undercooling. That resulted in fast crystallization kinetics which made it difficult to monitor the initial stages where the gel point occurs.

In this paper we report the structural and kinetic characteristics of evolving clusters during the early stages of crystallization, specifically at the critical gel state for low undercooling ($\Delta T = 15–23$ K). Real-time observation of melt crystallization of isotactic polypropylenes (iPP) was performed using SALS to measure in situ density and anisotropy fluctuations. Gel times t_c were obtained from recent rheological experiments on the same iPP sample.[5] We also used the extensive published DSC data on the growth of crystallinity of iPP,[15] which, however, needed to be extrapolated to the early stages of crystallization. DSC test runs at three temperatures ($T = 123.8$, 130, and 133 °C) showed that our iPP crystallized at the same rate as samples in ref 15. This allowed us to compare the time scales of crystallinity growth governed by Avrami time (from DSC), connectivity growth governed by gel time (from rheology), and evolution of clusters governed by characteristic times of structure development (from SALS).

Differential Scanning Calorimetry. Kinetics of crystallization at early and intermediate stages may be represented by the Avrami equation,[12−14] which originally was based on the formation of the nuclei of critical size and their subsequent growth (primary crystallization):

$$\frac{X(t)}{X_\infty} = 1 - e^{-(t/t_A)^N} \tag{1}$$

The Avrami equation is formally able to express the growth of bulk crystallintiy X, which is defined as mass fraction of crystalline phase in the polymer; X_∞ is the maximum attainable crystallinity at long times. N is the Avrami exponent, related to the crystal growth dimension, and t is the duration of crystallization experiment. The Avrami equation is commonly used much beyond the original Avrami model since it is able to express the shape of the measured $X(t)$ for a wide range of morphologies.

The Avrami time, t_A, is the time by which the relative degree of crystallinity $X/X_\infty = 1 - e^{-1} = 0.63$ has reached 63% of the final degree of crystallinity X_∞. Thus, t_A characterizes the growth of crystallinity. Its temperature dependence may be expressed as[5,6]

$$t_A = Ae^{-B\Delta T} \tag{2}$$

where $A = 3.0 \times 10^6$ s, $B = 0.237$ K^{-1} (from extrapolation of Kim's[15] results) and $A = 5.0 \times 10^6$ s, $B = 0.235$

K^{-1} (from extrapolation of our data). Experimental values of Avrami times and extrapolating graphs according to eq 2 are presented in Figure 3. We tested our sample in three selected DSC experiments and found good agreement with published DSC data; that justifies the use of Kim's data in our experiment. A most simple temperature dependence could be chosen here since ΔT needed to be small for slow crystallization.

Rheology. The physical gel point (formation of sample spanning network) is manifested in the slow power law dynamics of the shear relaxation modulus[32,33]

$$G(t) = St^{-n} \qquad \text{for } \lambda_0 < t < \lambda_{pg} \qquad (3)$$

where S is the gel stiffness, n is the relaxation exponent, and λ_0 is the crossover to short time dynamics (entanglements, glass transition modes). The longest relaxation time, λ_{pg}, is finite for physical gels in general; here we find that the lifetime of the crystal structure is much longer than the experimental time and set $\lambda_{pg} = \infty$.

In oscillatory shear the dynamic moduli at the gel point also follow power law behavior:

$$G'_c = \frac{G''_c}{\tan \delta} = S\Gamma(1 - n) \cos\frac{n\pi}{2}\omega^n \qquad \text{for } \omega < 1/\lambda_0 \quad (4)$$

A consequence of power law dynamics is a frequency-independent loss tangent

$$\tan \delta_c = \frac{G''_c}{G'_c} = \tan\frac{n\pi}{2} = \text{const} \qquad \text{for } \omega < 1/\lambda_0 \quad (5)$$

This provides the most reliable and generally valid method to determine the gel time and the parameters n and S.[16]

We characterized the rheological properties of the critical gel at low undercooling ΔT.[5,6] It was found that with increasing ΔT the relaxation exponent n decreases from 0.8 to 0.5, the gel stiffness increases from $\log S = 3.7$ to 4.4, and the gel time t_c decreases exponentially. Nucleation and crystallization kinetics may be compared to the rate of network formation by measuring the ratio of gelation time to Avrami time, t_c/t_A. This ratio depends on the activation energies to interconnect (gelation) and to crystallize (ordering). For iPP, this ratio is very low, $0.1 < t_c/t_A < 0.4$; i.e., gelation (connectivity growth) occurs at the very early stages of crystallization process.[5]

This raises basic questions about the underlying structure. How can it be that the growth rate of network formation is so much higher than the rate of bulk crystallization? What is the morphology of the sample spanning network structure?

This study was undertaken to see whether large structural units can be seen at the gel point and what the composition of these structured units might be. SALS is expected to answer some of these questions.

Experimental Section

We studied isotactic polypropylene (iPP) homopolymer from Fina Co. (referred to as sample B in ref 5). Molecular weights and polydispersity of the sample were measured using gel permeation chromatography (GPC) at Exxon Chemical, Baytown, TX. The sample was of a high molecular weight and high polydispersity: $M_n = 84.168 \times 10^3$, $M_w = 351.163 \times 10^3$, $M_z = 1004.781 \times 10^3$, $M_w/M_n = 4.17$, and $M_z/M_w = 2.86$. Samples (50–100 μm thick) were prepared by melt pressing an iPP pellet between two cover glasses at 210 °C for 20 min under vacuum in a carver laboratory press. Subsequently, the specimens were rapidly transferred into a light-scattering hot stage set at a temperature $T_{exp} = 140$, 144, and 148 °C. The nominal melting temperature for the samples was measured as peak in the DSC endotherm at $T_{melt} = 163$ °C.

The light scattering measurements were carried out under both Hv (crossed) and Vv (parallel) polarization modes with the use of a vertical SALS apparatus which consists of a 10 mW He/Ne laser ($\lambda = 632.8$ nm), polarizer, analyzer, and CCD camera (Sanyo Co) as the detector. A more complete description of the SALS instrument is given elsewhere.[17] Scattering images were recorded at variable intervals, depending on experimental conditions, and then digitized and stored for later analysis. Hv and Vv patterns were corrected for intensity variations and distortions of the image arising from the angle and distance of the camera. Corrections for refraction, reflection, and multiple scattering were not made. The samples were sufficiently thin so that loss of scattered energy from the scattered beam through secondary scattering may be negligibly small.[18] Transmitted intensity was monitored simultaneously with intensities of scattered light under both parallel and crossed polarizers.

Small-Angle Light Scattering Analysis. Theory of light scattering behavior is based on a model of the morphological characteristics. The analysis here is based on the assumption that the polymer develops spherulites which are understood as three-dimensional, spherically symmetrical clusters of crystalline and noncrystalline polymer. The simplest model of a spherulite is that of a uniformly isotropic sphere of radius R.[19] A more physically realistic spherulite model considers isolated anisotropic spheres in an isotropic medium. Due to the ordered arrangement of anisotropic crystallites along the radii, these spherulites have different radial and tangential refractive indices. Under these assumptions, Stein and Rhodes[20] derived the general equations for the Hv and Vv intensities of the scattered light

$$I_{Hv} = C_1 V_{sph}{}^2\left(\frac{3}{u^3}\right)^2\left[(\alpha_t - \alpha_r)\cos^2\frac{\theta}{2}\sin\mu\cos\mu \times\right.$$
$$\left.(4\sin u - u\cos u - 3Si(u))\right]^2 \quad (6)$$

$$I_{Vv} = C_1 V_{sph}{}^2\left(\frac{3}{u^3}\right)^2\left[(\alpha_t - \alpha_r)(2\sin u - u\cos u -\right.$$
$$Si(u)) + (\alpha_r - \alpha_0)(Si(u) - \sin u)) +$$
$$\left.(\alpha_t - \alpha_r)\cos^2\frac{\theta}{2}\cos^2\mu(4\sin u - u\cos u - 3Si(u))\right]^2 \quad (7)$$

where C_1 is a constant, V_{sph} is the volume of a single sphere, $u = (4\pi R/\lambda)\sin(\theta/2) = qR$ is the shape factor, q is the scattering vector, λ is the wavelength of light, α_t and α_r are the tangential and radial polarizabilities of the sphere, respectively, α_0 is the polarizability of the surrounding medium, and θ and μ are the polar and azimuthal scattering angles. The polarizability is a microscopic electric property of dielectric medium which relates the applied external electric field E with induced polarization (electric dipole density) $\mathbf{P} = \alpha\mathbf{E}$.

$Si(u)$ is a short symbol for

$$Si(u) \equiv \int_0^u \frac{\sin X}{X}X \quad (8)$$

The $(\sin \mu \cos \mu)^2$ term in eq 6 leads to a 4-fold symmetric scattering pattern with intensity maxima at azimuthal angles $\mu = \pi k/4$ where k is an odd number. According to eq 6, the Hv intensity depends directly upon the anisotropy of the spherulite and is zero when $\alpha_t = \alpha_r$. In eq 7 the first two terms are independent of μ (circularly symmetrical), whereas the third term depends on $\cos^2 \mu$. This third term leads to 2-fold symmetry with intensity maxima at $\mu = \pi k$, where k is a
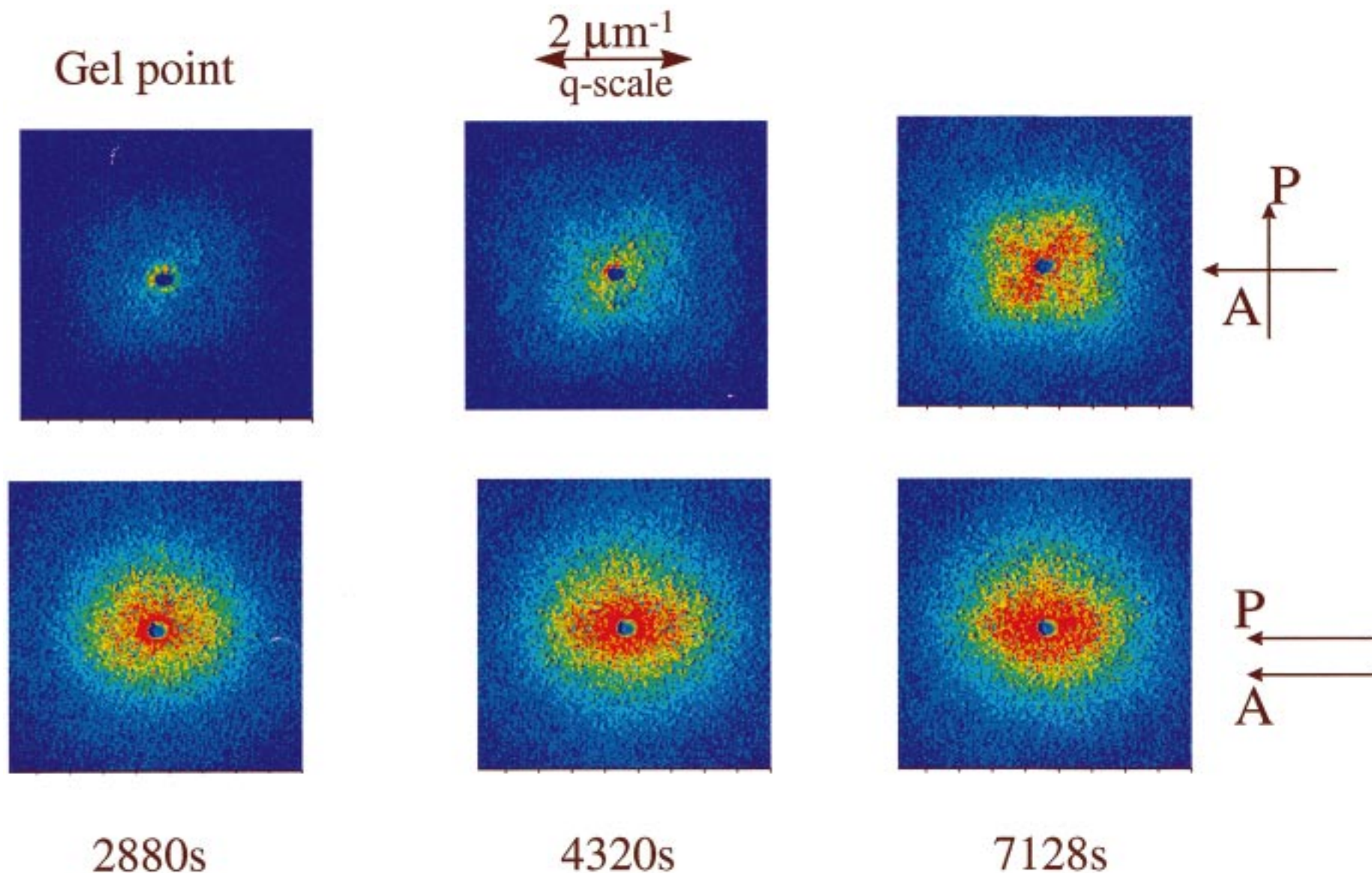
Figure 1. Hv (crossed polarizers) and Vv (parallel polarizers) patterns during crystallization of iPP at 140 °C. Melt background contribution has been subtracted.
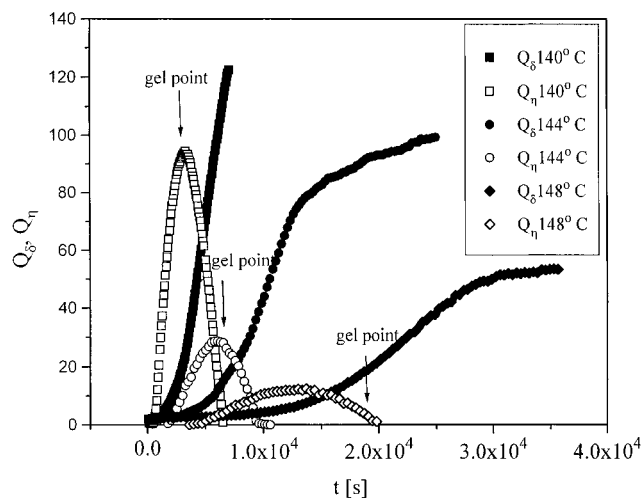
Figure 2. Time variation of Q_δ and Q_η invariants during crystallization at three different temperatures. Gel times and Avrami times are shown by the arrows. Direction of integration was $\mu = 45°$ for Q_δ and $\mu = 0°$ for Q_η.
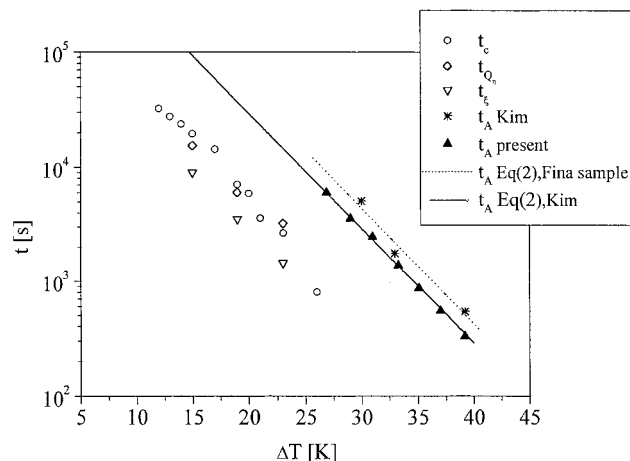
Figure 3. Semilogarithmic plot of characteristic times from rheology (t_c) and SALS (t_{Q_η}, t_ξ) versus degree of undercooling: t_{Q_η} corresponds to the moment of the maximum in density fluctuation Q_η; t_ξ corresponds to moment of the maximum in correlation length ξ. t_A corresponds to Avrami time: stars stand for time from our DSC data, and triangles show the times obtained using Kim's data. The lines represent Avrami times t_A (ΔT) estimated according to eq 2: $A = 3.0 \times 10^6$ s, $B = 0.237$ K^{-1} (solid line, Kim's[15] data), and $A = 5.0 \times 10^6$ s, $B = 0.235$ K^{-1} (dashed line, our sample).

positive integer. The first two terms in eq 7 depend on α_0 (which is the isotropic polarizability of the surroundings), whereas the third term depends on the anisotropy of the spherulite ($\alpha_t - \alpha_r$).

Stein and Yoon[21] generalized eqs 6 and 7 for a collection of randomly located spherulites. The polarizability of the surroundings is then given by

$$\alpha_0 = \Phi_d[(\alpha_r + 2\alpha_t)/3 + (1 - \Phi_d)\alpha_{am}] \quad (9)$$

where Φ_d is the volume fraction of spherulites and α_{am} is the polarizability of the amorphous phase.

The theory, however, is limited to perfect spherulites where the crystallite orientation and the resultant optic axis make a constant angle with the spherulite radius. Real spherulites may be disordered and will have an ill-defined geometry. For such systems, statistical (Debye–Bueche type) approaches based on correlation functions are more realistic.[22,23]

In this paper the quantitative analysis of scattered light is based on the statistical approach for anisotropic systems developed by Stein and Wilson.[24] The analysis does not depend on the geometry of the scattering objects but depends only on the contrast causing the scattering. It postulates random orientation fluctuations where the probability of a crystallite optic axis at two different positions being parallel depends only on their separation and not on the angle that the optic axes make with respect to the interconnecting vector. This implies spherical symmetry of correlated regions and leads to circular symmetry of the scattered intensities about the incident beam. The angular distribution of depolarized scattering intensity, I_{Vv}, and polarized scattering intensity, I_{Hv}, are then[24]

$$I_{Vv} - (4/3)I_{Hv} \propto \langle \eta^2 \rangle \int_0^\infty \gamma(r) \frac{\sin qr}{qr} 4\pi r^2 \, dr \quad (10)$$

$$I_{Hv} \propto \langle \delta^2 \rangle \int_0^\infty f(r) \frac{\sin qr}{qr} 4\pi r^2 \, dr \quad (11)$$

where $\langle \eta^2 \rangle$ is the mean-square density fluctuation and $\gamma(r) = \langle \eta_i \eta_j \rangle / \langle \eta^2 \rangle$ is the correlation function of the density fluctuation, where $\eta_j = \alpha_j - \langle \alpha \rangle$ is the polarizability fluctuation at position i. $\langle \delta^2 \rangle$ is the mean of the squared anisotropy. The optical anisotropy of the particle δ is defined as the difference between two main polarizabilities of the particle. δ is the optical anisotropy of the uniaxial volume element defined as the difference in its principal polarizabilities. $f(r)$ is the correlation function of the orientation fluctuations:

$$f(r) = [3\langle \cos^2 \theta_{ij} \rangle_r - 1]/2 \quad (12)$$

where θ_{ij} is the angle between optic axes of the i and j volume elements separated by a distance r. $f(r)$ reduces to zero for large r or when θ_{ij} is random, i.e., $\langle \cos^2 \theta_{ij} \rangle_r = 1/3$.

I_{Hv} arises from orientation fluctuations while I_{Vv} arises from both orientation and density fluctuations. For $\delta = 0$, $I_{Hv} = 0$ and I_{Vv} of eq 12 reduces to the Debye–Bueche[22,23] result for a random two-phase system

$$I_{Vv} = C_2 \langle \eta^2 \rangle \int_0^\infty \gamma(r) \frac{\sin qr}{qr} 4\pi r^2 \, dr \quad (13)$$

where $\gamma(r)$ has the simple exponential form $\gamma(r) = e^{-r/\xi}$. The correlation length ξ is a measure of the spatial size of fluctuations, and C_2 is a constant. Combination of eqs 12 and 13 gives

$$I(q) = \frac{A}{(1 + \xi^2 q^2)^2} \quad (14)$$

where A is a constant. The Debye–Bueche type plots ($I(q)^{-1/2}$ vs q^2) should show a linear dependence

$$I^{-1/2} = \frac{1}{A^{1/2}} + \frac{\xi^2}{A^{1/2}} q^2 \quad (15)$$

Then, the square of the correlation length ξ^2 is found as ratio of a slope to intercept.

Crystallization kinetics is conveniently described in terms of the invariants Q_η and Q_δ,[25] which are defined as integrated scattering intensities:

$$Q_\eta = \int_0^\infty (I_{Vv} - (4/3)I_{Hv})q^2 \, dq \propto \langle \eta^2 \rangle \propto$$
$$\Phi_d(1 - \Phi_d)(\alpha_d - \alpha_0)^2 \quad (16)$$

$$Q_\delta = \int_0^\infty I_{Hv} q^2 \, dq \propto \langle \delta^2 \rangle \propto \Phi_d \delta_d^2 \quad (17)$$

where Φ_d is the volume fraction of the growing clusters and $\alpha_d = (\alpha_1 + 2\alpha_2)/3$ and α_0 are the average polarizabilities of the growing clusters and the melt, respectively; $\delta_d = \Phi_c(\alpha_1 - \alpha_2)f$ is the optical anisotropy of the clusters, Φ_c is the volume fraction crystallinity within the clusters, $(\alpha_1 - \alpha_2)$ is the

intrinsic anisotropy of the crystallites in the growing clusters, and f is the orientation factor describing the orientation of the optical axes of the crystallites with respect to the radius of the spherulite. Hence, from the temporal variation of $\langle \eta^2 \rangle$ and $\langle \delta^2 \rangle$, the crystallization kinetics can be probed in terms of Φ_d and Φ_c.

It needs to be mentioned that the Stein–Wilson approach is adequate only at early stages of crystallization where the random orientation function approximation holds. At later stages the correlation may become nonrandom if crystallization occurs through unidirectional growth mechanisms;[26,27] i.e., crystals form rodlike and then sheaflike clusters. This leads to a noncircular type of Hv scattering, and two-dimensional integration over both angles Θ and μ is required for interpretation of the Q_δ invariant.

Results and Discussion

Scattered Light. Typical SALS patterns during the course of crystallization are shown in Figure 1. The gel point occurs during the early stages of crystallization at $t \approx 2700$ s for $T = 140$ °C from rheological measurements, and the Vv pattern is intense and circularly symmetric due to the relatively large isotropic terms in eq 7. The corresponding Hv pattern is much less intense, and it follows from eq 6 that $\alpha_t - \alpha_r \approx 0$ since clusters at the gel point have very low crystallinity. At late stages, patterns show an increase in the intensity in both modes as well as the development of 2-fold and 4-fold symmetry in the Vv and Hv modes, respectively. According to eqs 6 and 7, pronounced dependence upon azimuthal angle μ means that *superstructures* with high anisotropy ($\alpha_t - \alpha_r$) have developed. However, patterns at these late stages show excess scattering so that intensities do not drop to zero at $\mu = 0°$ and $\mu = 90°$ for the Hv mode and at $\mu = 90°$ for the Vv mode, as predicted by eqs 6 and 7 for idealized spherulites. The observed excess scattering is indicative of imperfect structures: truncated polygonals[28] or spherulites with internal disorder.[29] We have no means, however, at present to separate contributions of each of these models, and a statistical approach should be used for quantitative analysis (eqs 16 and 17).

Calculated values of Q_η and Q_δ at 140, 144, and 148 °C are plotted as a function of the crystallization time in Figure 2. (Integration according to eq 16 was performed at $\mu = 0°$ and according to eq 17 at $\mu = 45°$.) During the induction period, growing clusters are too small to be detected by SALS. Both invariants show simultaneous onset of growth after the induction time. The evolution of $\langle \eta^2 \rangle$ is characterized by a maximum, which by eq 16 occurs when Φ_d attains 0.5; i.e., growing clusters occupy 50% of the total volume. We define the time of this maximum t_{Q_η}. For $t > t_{Q_\eta}$, the mean-square density fluctuation $\langle \eta^2 \rangle$ and Q_η decrease as clusters become overlapping. The important experimental result is that at later times $\langle \eta^2 \rangle$ and Q_η not only decrease but reach zero. This means that clusters become volume filling (i.e., $\Phi_d \rightarrow 1$) and the average polarizability of the surrounding matrix (which now consists of similar crystalline clusters) becomes close to that of clusters, $\alpha_0 \sim \alpha_d$ (see eq 9).

The characteristic times t_{Q_η} are plotted versus undercooling temperature in Figure 3 and are very close to the gel times determined in our rheological testing for this sample but are much shorter than the corresponding Avrami times.[5] At the moment of the liquid–solid transition, clusters impinge; i.e., interconnected network arises. As t_c are very close to t_{Q_η}, we can say that the
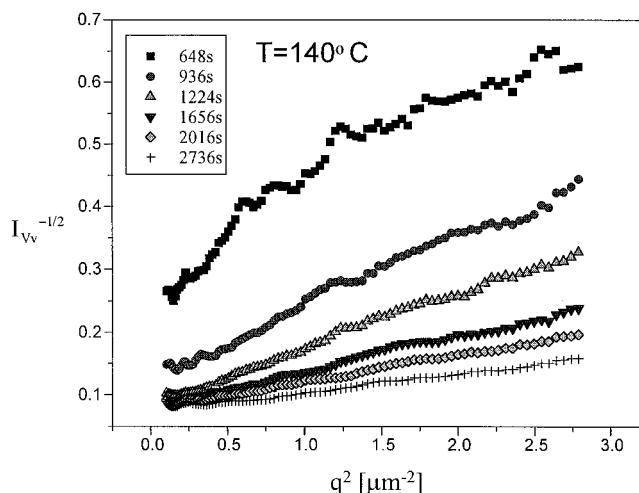
Figure 4. Debye–Bueche plots at different times during isothermal ($T = 140$ °C) crystallization. Times are depicted by different symbols.

liquid–solid transition occurs very close to the instant of the maximum of density fluctuation in the system. In terms of the presented above approach (see eq 16), it occurs when the volume fraction of the crystalline cluster Φ_d attains about 0.5.

The time variation of $\langle \delta^2 \rangle$ in Figure 2 corresponds to the development of orientation fluctuations. It is important to emphasize that at the characteristic time $t = t_{Q_\eta}$, when the Q_η invariant reaches its maximum, the value of the Q_δ invariant is very low. This implies, according to eq 17, low optical anisotropy δ_d and volume fraction crystallinity Φ_c of the cluster. This strongly supports the result from our rheological data that nearly all of the crystallization occurs on the template of the solid structure of the critical gel.[5,6] The large increase in Q_δ after solidification suggests that most of the material crystallizes during this late stage.

To understand the behavior of the Q_δ invariant, we will define "primary" and "secondary" crystallization. We define primary crystallization as the radial growth of clusters and fibrous crystalline "strands" governed by radial growth rate. This process is responsible for interconnected network formation (gelation) and is manifested experimentally in t_c. The strong increase in the Q_δ invariant after the gel point (see Figure 2) suggests the presence of secondary crystallization. We define secondary crystallization as a process of internal crystallization and ordering which proceeds within the impinged clusters. This process is responsible for the growth of crystallinity and is manifested in t_A.

The circular symmetry of the SALS patterns at early stages of growth in Figure 1 suggests that one can apply a modification of the Debye–Bueche[22,23] approach for scattering from random heterogeneous media in order to estimate the length of the growing fluctuation ξ. We need to keep in mind that the term "correlation" length was used in the Introduction to describe the distance at which molecular motions are correlated. In this section correlation length defines the inhomogeneity length of the crystalline or amorphous phase.

The Debye–Bueche plots ($I(q)^{-1/2}$ against q^2) for circularly averaged Vv intensities are shown in Figure 4 for the intermediate angular range. Experimental curves can be well approximated by linear dependencies which confirms the validity of the Debye–Bueche approach. Correlation length is determined as a square
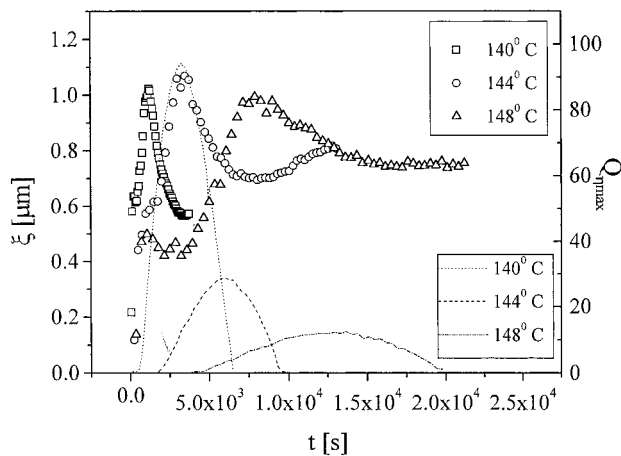
Figure 5. Time variation of the correlation length ξ (symbols) and Q_η invariant (dashed and dotted lines) at three different temperatures. The maximum in ξ occurs earlier than the maximum in Q_η. The time scale is the same for both plots.

root of the slope-to-intercept ratio (see eq 15). For the three studied temperatures, ξ increases, attains a maximum of about ~ 1 μm, and then decreases to a constant value of about 0.6–0.7 μm (Figure 5). This observation can be rationalized by following the approach of Debye[23,29,30] for a random dispersion of two phases of volume fractions ϕ_1 and ϕ_2 and definite composition for which the ratio of the interphase surface area S to the volume V is related to the correlation distance by

$$S/V = 4\phi_1\phi_2/\xi \tag{18}$$

The average chord lengths of the two phases are $\langle l_1 \rangle = \xi/\phi_2$ and $\langle l_2 \rangle = \xi/\phi_1$, from which it follows that

$$1/\langle \xi \rangle = \phi_2/\langle l_1 \rangle + \phi_1/\langle l_2 \rangle \tag{19}$$

The harmonic average of the dimensions of the phases is given by $\langle \xi \rangle$, and $\langle l_i \rangle$ is the mean dimension of a given phase (phase 1 is amorphous and phase 2 is crystalline). During the early stages of growth (i.e., $\phi_1 \rightarrow 1$, $\phi_2 \rightarrow 0$), $\langle \xi \rangle$ is on the order of the size of the superstructures, $\langle \xi \rangle \sim \langle l_2 \rangle \sim \langle R \rangle$. The correlation length passes through a maximum when the volume fraction of crystalline phase ϕ_2 is about 0.5. At this volume fraction $1/\langle \xi \rangle = 0.5(1/\langle l_1 \rangle + 1/\langle l_2 \rangle)$, so $\langle \xi \rangle$ is a characteristic length scale associated with the clusters. For larger values of ϕ_2, $\langle \xi \rangle$ is a measure of the amorphous regions, i.e., $\langle \xi \rangle \sim \langle l_1 \rangle$. Figure 5 shows the continuous decrease of $\langle \xi \rangle$ to 0.6–0.7 μm. This suggests that the average size of the amorphous regions decreases; i.e., primary crystallization is still occurring, and the crystalline clusters are continuing to grow. We define t_ξ as the time when the correlation length $\langle \xi \rangle$ passes through a maximum. It seems physically reasonable that t_ξ is shorter than t_{Q_η} and t_c (see Figures 3 and 5) because clusters are still growing until ξ reaches its constant low value ξ_{min}. This indicates that amorphous regions stopped decreasing in size and primary crystallization is complete.

Using the increasing values of the correlation length at early stages, when it is of the order of the size of clusters $\langle \xi \rangle \sim R$ in Figure 5, we followed the growth of the isotropic cluster in Figure 6. Figure 6 shows that the size of occurring fluctuations of about 1 μm. (The maximum size of the growing fibrous cluster may be much greater.) Similar values of R have been reported
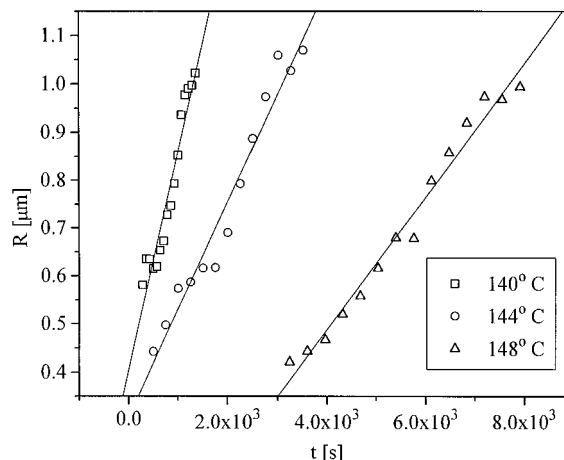
Figure 6. Time variation of the radius of the isotropic domain at early stages at three different temperatures $T = 140$, 144, and 148 °C.
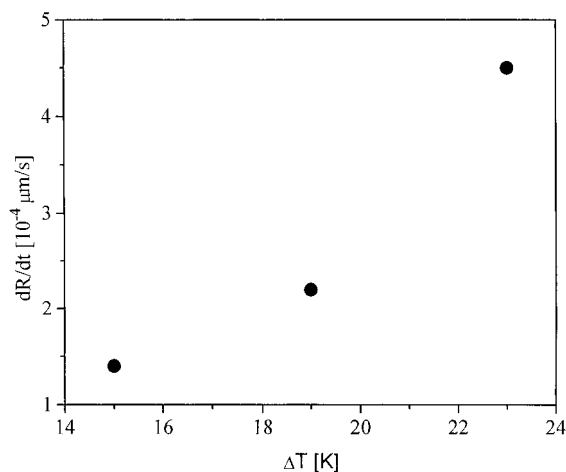
Figure 7. Growth rate of the size of fluctuation associated with cluster dR/dt versus degree of undercooling.

for iPP at early stages by Okada et al.[10] The slope of the linear approximation gives the growth rate $G_\eta = dR/dt$ of the size of fluctuation. G_η is plotted versus undercooling in Figure 7 and shows a typical increase at higher ΔT. This reflects the higher growth rate and smaller cluster size with the increase of undercooling due to fast crystallization kinetics.

Figure 8 shows the relative degree of crystallinity versus relative time t/t_A according to eqs 1 and 2. Normalization of the time axes by t_A reduces the conventional Avrami plots to a single curve (solid line in Figure 8). Experimental points in Figure 8 represent the relative crystallinity of our iPP samples at characteristic times t_Q, t_ξ, and t_c for various undercoolings. The plot clearly shows that, according to rheology/DSC, solidification occurs at a critical relative degree of crystallinity X_c/X_∞ less than 3%; according to SALS/DSC, the maximum in the density fluctuation occurs at relative crystallinity less than 2%, and the correlation length ξ passes through its maximum at $X_c/X_\infty \sim 0.1\%$. Low anisotropy and internal crystallinity of growing clusters at early stages suggest that they may grow as anisometric crystallites, which form an interconnected network of fibrous crystals. These crystals are themselves anisotropic, but since their fraction is low, the anisotropy of the cluster is also low. Olley et al.,[27] studying iPP showed, that at very low undercooling the
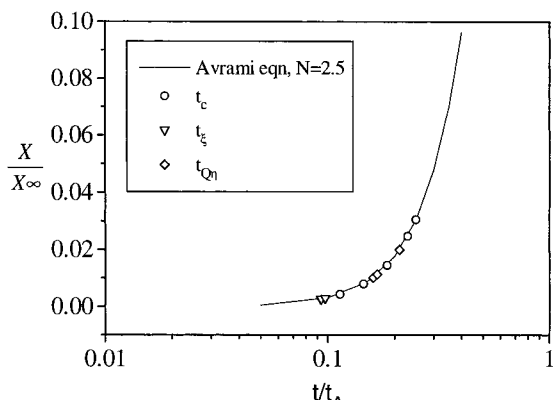
Figure 8. Relative degree of crystallinity versus relative time t/t_A according to Avrami eq 1 with the use of isothermal DSC data (by Kim et al.[15] and our own), solid line. Points represent the relative crystallinity of iPP sample at the relative times t_c/t_A (critical gel), $t_{Q\eta}/t_A$ (maximum Q_η), and t_ξ/t_A (maximum ξ).

first growing objects are anisometric sheaflike clusters which grow unidirectionally.

Transmitted Light. The appearance of crystals strongly affects the transmittance of polarized light in two ways: turbidity arises from the loss of intensity from the transmitted beam due to scattering from optically heterogeneous clusters, and birefringence in crossed polars arises from anisotropic clusters with uniform orientation of optic axes. Both physical phenomena (turbidity and birefringence) may be additionally affected (masked) by artifact "forward scattering" from big clusters entering the detector. The problem has been studied theoretically and experimentally.[31]

Morphology development during crystallization was probed by monitoring transmittance in both Hv and Vv modes. No correction for multiple scattering was attempted. The transmitted intensity under Vv mode I_{trVv} is related to the turbidity τ of the sample by

$$I_{trVv} = I_0 e^{-\tau h} \qquad (20)$$

where I_0 is the intensity transmitted without the sample and h is the sample thickness. Turbidity τ is a measure of total scattering intensity.

The intensity of the monochromatic light transmitted through a thin film between crossed polarizers I_{trVv} is a measure of the degree of uniaxial order in the arrangement of the optically anisotropic elements in the sample. Generally I_{trVv} is a function of $\sin^2 2\varphi_i$ and Δ_i^2, where φ_i is the angle between the optical axis of the ith anisotropic element with the polarization direction and Δ_i is the optical phase difference of the ith element.

In the simplest idealized case of unidirectional orientation of anisotropic elements (i.e., $\varphi = $ const), the intensity is given by

$$I_{trHv} = \frac{I_0}{2}\sin^2(2\varphi)\sin^2\left(\frac{\Delta}{2}\right) \qquad (21)$$

where $\Delta = (2\pi h/\lambda)(n_e - n_0)$ is the total optical retardation of the layer with thickness h, $n_e - n_0$ is the birefringence of the material, and I_0 is the intensity transmitted through polarizer.

In Figure 9 the change in the scattered and transmitted intensities I_{scatHv} and I_{trHv} under crossed polarizers is shown in the course of isothermal crystallization of iPP. While the scattered intensity increases in time and reaches its highest value at late stages, the transmitted
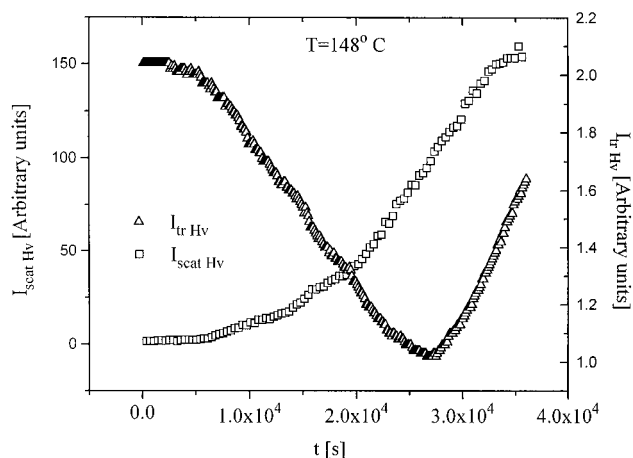
Figure 9. Time variation of transmitted I_{trHv} and scattered I_{scatHv} intensities in crossed polarizers during isothermal crystallization at 148 °C.
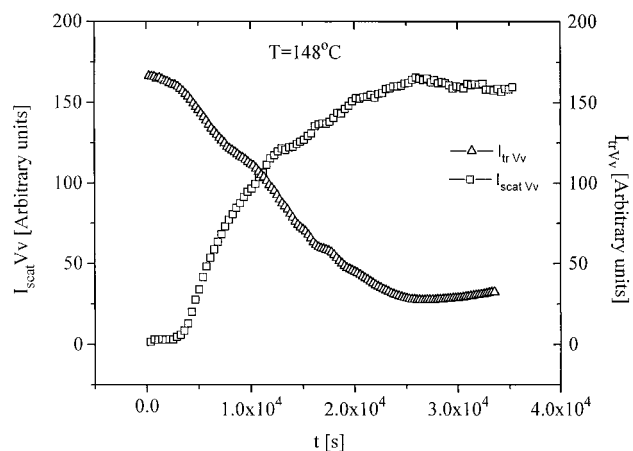
Figure 10. Time variation of transmitted I_{trVv} and scattered I_{scatVv} intensities in parallel polarizers during isothermal crystallization at 148 °C.

intensity is very weak, practically negligible (2 orders of magnitude lower than I_{trVv}); it decreases in the course of crystallization and shows a well-pronounced minimum at the late stage. Such behavior indicates low uniaxial ordering which decreases even further during crystallization. This is typical for evolving spherically symmetric or disordered structures with no macroscopic orientation of the optical axes. The origin of the minimum in I_{trHv} (Figure 9) is not clear. We attribute it to intense forward scattering from large mature spherulites at the late stages. As the spherulite size increases, the scattering pattern contracts toward smaller scattering angles, and more of the scattered light is able to enter the photodiode aperture.

Figure 10 shows the changes in the scattered and transmitted intensities in the Vv mode I_{scatVv} and I_{trVv} during crystallization. The values of transmitted intensity in the Vv mode I_{trVv} are 2 orders of magnitude higher than I_{trHv} and characterize the turbidity of the system (see eq 20). The growth of crystalline clusters leads to an increase in scattering corresponding to a greater loss of intensity from the transmitted beam as represented by eq 20. At the start of crystallization the system is in the state of transparent melt, which is reflected in high values of transmitted intensity I_{trVv}. As crystalization develops and crystals are growing, the system becomes more and more opaque. I_{trVv} constantly decreases with increasing turbidity and levels off in the

late stage. A weak increase in I_{trVv} at the latest stage may be attributed to the intense forward scattering from large spherulites.

Conclusions

Small-angle light scattering (SALS) shows that large clusters exist at the gel point. The clusters are mostly amorphous. SALS is able to measure the growth of density fluctuations and orientation fluctuations. The maximum in density fluctuation is very close to the rheologically obtained gel point. This occurs when clusters have impinged, $\Phi_d = 0.5$. Orientation fluctuations develop much more slowly and appear at much later stages of the crystallization process. The gel point clusters are of unknown low anisotropic structure and are of the order of 1 μm in size. At late stages, SALS patterns display 2-fold and 4-fold symmetry in Vv and Hv modes, respectively, indicating the development of anisotropic structures. The growth of crystalline clusters leads to a strong increase in turbidity (i.e., decrease in light transmission in the Vv mode).

The early development of a sample spanning network at very low crystallinity has significant implication for polymer processing. The heterogeneous microstructure (large density fluctuation, low crystal fraction) very strongly depends on stereoregularity of the molecules which explains the extreme sensitivity of processing to small changes in molecular structure. More studies are needed on the early stages of evolving microstructure and on possibilities of controlling structure development during processing.

References and Notes

(1) Mandelkern, L. *Crystallization of Polymers*; McGraw-Hill: New York, 1993.
(2) Fatou, J. G. Crystallization Kinetics. In *Encyclopedia of Polymer Science and Engineering*; Suppl. Vol.; J. Wiley: New York, 1989.
(3) Zachmann, H. G.; Wutz, C. In *Crystallization of Polymers*; Dosiere, M., Ed.; Kluwer Academic Pub.: Boston, 1993.
(4) Phillips, P. J. Polymer Crystals. *Rep. Prog. Phys.* **1990**, *53*, 549.
(5) Pogodina, N. V.; Winter, H. H. *Macromolecules* **1998**, *31*, 8164.
(6) Schwittay, C.; Mours, M.; Winter, H. H. *Faraday Discuss.* **1995**, *101*, 93.
(7) Price, F. In *Growth and Perfection of Crystals*; Doremus, Roberts, Turnbull, Eds.; John Wiley and Sons: New York, 1958.
(8) Stein, R. S.; Ree, M.; Kyu, T. *J. Polym. Sci., Polym. Phys. Ed.* **1987**, *25*, 105.
(9) Stein, R. S.; Cronauer, J.; Zachmann, H. G. *J. Mol. Struct.* **1996**, *383*, 19.
(10) Okada, T.; Saito, H.; Inoue, T. *Macromolecules* **1992**, *25*, 1908.
(11) Akpalu, Y.; Hsiao, B. S.; Stein, R. S.; Muthukumar, M., personal communication.
(12) Avrami, M. *J. Chem. Phys.* **1939**, *7*, 1103.
(13) Avrami, M. *J. Chem. Phys.* **1940**, *8*, 212.
(14) Avrami, M. *J. Chem. Phys.* **1941**, *9*, 177.
(15) Kim, C. Y.; Kim, Y. C.; Kim, S. C. *Polym. Eng. Sci.* **1993**, *33*, 1445.
(16) Holly, E. E.; Venkataraman, S.; Chambon, F.; Winter, H. H. *J. Non-Newt. Fluid Mech.* **1988**, *27*, 17.
(17) Van Egmond, J. W.; Werner, D. E.; Fuller, G. G. *J. Chem. Phys.* **1992**, *96*, 7742.
(18) Stein, R. S.; Keane, J. J. *J. Polym. Sci.* **1955**, *17*, 21.
(19) Guinier, A.; Fournet, G.; Walker, C.; Yudowitch, K. *Small Angle Scattering of X-rays*; Wiley: New York, 1955.
(20) Stein, R. S.; Rhodes, M. B. *J. Appl. Phys.* **1873**, *31*, 1960.
(21) Yoon, D. Y.; Stein, R. S. *J. Polym. Sci., Polym. Phys. Ed.* **1974**, *12*, 735.
(22) Debye, P.; Bueche, A. M. *J. Appl. Phys.* **1949**, *20*, 518.
(23) Debye, P.; Anderson, H. R.; Brumberger, H. *J. Appl. Phys.* **1957**, *28*, 679.
(24) Stein, R. S.; Wilson, P. R. *J. Appl. Phys.* **1962**, *33*, 1914.
(25) Koberstein, J.; Russell, T. P.; Stein, R. S. *J. Polym. Sci., Polym. Phys. Ed.* **1979**, *17*, 1719.
(26) Lotz, B.; Wittman, J. C. *Polym. Eng. Sci.* **1986**, *24*, 1541−1558.
(27) Olley, R. H.; Bassett, D. C. *Polymer* **1989**, *30*, 399−409.
(28) Stein, R. S.; Picot, C. *J. Polym. Sci., Part A-2* **1970**, *8*, 2127.
(29) Stein, R. S. Small Angle Light Scattering From the Polymeric Solid State. In *Crystallization of Polymers*; Dosiere, M., Ed.; Kluwer Academic Pub.: Boston, 1993; p 109.
(30) Kratky, O. *Pure Appl. Chem.* **1966**, *12*, 483.
(31) Clough, S.; Rhodes, M. B.; Stein, R. S. *J. Polym. Sci., Part C* **1967**, *18*, 1−32.
(32) Chambon, F.; Winter, H. H. *Polym. Bull.* **1985**, *13*, 499. Winter, H. H.; Chambon, F. *J. Rheol.* **1986**, *30*, 367. Chambon, F.; Winter, H. H. *J. Rheol.* **1987**, *31*, 683.
(33) Winter, H. H.; Mours, M. *Adv. Polym. Sci.* **1997**, *134*, 165.